JMEPEG (2005) 14:654-665
DOI: 10.1361/105994905X64585

1059-9495/$19.00

Characterization of N-Doped Polycrystalline Diamond Films Deposited on Microgrinding Tools

M.J. Jackson and W. Ahmed

(Submitted June 20, 2005; in revised form July 22, 2005)

Chemical vapor deposited diamond films have many industrial applications but are assuming increasing importance in the area of microengineering, most notably in the development of diamond coated microgrinding tools. For these applications the control of structure and morphology is of critical importance. The crystallite size, orientation, surface roughness, and the degree of sp^3 character have a profound effect on the tribological properties of the films deposited. In this article, we present experimental results on the effects of nitrogen doping on the surface morphology, crystallite size, and wear of microgrinding tools. The sp^3 character optimizes at 200 ppm nitrogen, and above this value the surface becomes much smoother and crystal sizes decrease considerably. Fracture-induced wear of the diamond grain is the most important mechanism of material removal from a microgrinding tool during the grinding process. Fracture occurs as a consequence of tensile stresses induced into diamond grains by grinding forces to which they are subjected. The relationship between the wear of diamond coated grinding tools, component grinding forces, and induced stresses in the model diamond grains is described in detail. A significant correlation was found between the maximum value of tensile stress induced in the diamond grain and the appropriate wheel-wear parameter (grinding ratio). It was concluded that the magnitude of tensile stresses induced in the diamond grain by grinding forces at the rake face is the best indicator of tool wear during the grinding process.

Keywords characterization, cutting tools, diamond, microengineering, surface engineering

1. Introduction

Diamond has a unique combination of excellent physical and chemical properties, which makes it ideal for numerous applications (Ref 1-3). It can be used in biomedical components, cutting tools, optical components, microelectronic circuits, and thermal management systems. A number of methods were investigated to deposit diamond in thin form to various substrates, the most common being silicon and tungsten carbide cemented with a small amount of cobalt metal (Ref 4-6). Arguably, the most successful method of depositing polycrystalline films of diamond is chemical vapor deposition (CVD). In this study, we investigated a variant of the basic CVD process known as hot-filament CVD for the deposition of diamond. It is generally agreed that the properties of the films, such as morphology, quality, and adhesion determine the suitability for use in a particular application (Ref 7). In the case of microgrinding tools, extremely small particles of diamond that are blocky in form are required so that cutting of metals and other materials can be performed with relative ease. Both the diamond nucleation stage and the CVD process conditions critically affect the structure and morphology. Abrasion of the

M.J. Jackson, Center for Advanced Manufacturing, Purdue University, College of Technology, West Lafayette, IN 47907-2021; and **W. Ahmed,** Department of Chemistry & Materials, Dalton Research Institute, Manchester Metropolitan University, Chester Street, Manchester M1 5GD, UK. Contact e-mail: jacksomj@purdue.edu.

Nomenclature

a	diamond wedge half-space, mm
a, b, c, d	constants related to stress functions associated with a diamond wedge that has distributed loading
C	constant
F_t	tangential force, N
F_Y	equivalent tangential grinding force, N
F_Z	equivalent normal grinding force, N
G	grinding ratio, mm^3/mm^3
n	force multiplier, or coefficient
P	point load, N
r	radial polar coordinate
t	thickness of diamond wedge, mm
V_S	volume of diamond surface layer removed, mm^3
V_W	volume of workpiece material removed, mm^3
β	rake angle of wedge (diamond grain)
ϕ	stress function
θ	angular polar co-ordinate
μ	coefficient of friction
σ_1	principal stress, N/mm^2
σ_3	principal stress, N/mm^2
σ_c	compressive strength of diamond, N/mm^2
σ_r	radial stress, N/mm^2
σ_t	tensile strength of diamond, N/mm^2
$\sigma\theta$	circumferential, or hoop stress, N/mm^2
$\tau_r\sigma$	shear stress, N/mm^2
ω	angle between point load and apex of diamond wedge

substrate material with diamond powder prior to deposition is commonly used to enhance the diamond nucleation density (Ref 8-10). However, such abrasion methods damage the surface in a poorly defined manner. Thus, more controlled methods of nucleation such as biasing prior to standard CVD are becoming increasingly common (Ref 11, 12) and can even enable heteroepitaxial growth of diamond films (Ref 13, 14). The gas-phase environment during deposition also affects the quality and morphology of the resulting diamond films. The addition of nitrogen (Ref 15, 16), boron (Ref 17), and phosphorus (Ref 18) containing gases to the standard methane/hydrogen gas mixtures can radically change crystal grain size and its faceting. The effect of changing the stoichiometric balance of the mixture of gases has a significant effect on the development of wear in micro grinding tools.

Wear mechanisms in microgrinding tools appear to be similar to that of single-point cutting tools, the only difference being the size and nature of swarf particles generated. Microgrinding tools contain very small sharp abrasive grains with blunted cutting edges (known as wear flats) and diamond grains with sharp cutting edges that are released from the grinding tool before they have a chance to remove material from the workpiece. The general form of the wear curve is similar to that of a single-point cutting tool. The wear behavior observed is similar to that found in other wear processes; high initial wear followed by steady-state wear. A third accelerating wear regimen usually indicates the occurrence of catastrophic wear of the tool. This type of wear is usually accompanied by thermal damage to the surface of the machined workpiece, which reduces fatigue strength and the life of the component. The performance index used to characterize wear resistance is the grinding ratio, or G-ratio, and is expressed as the ratio of the change in volume of the workpiece ground Δv_w to the change in the volume of the surface of the tool removed Δv_s and is shown in Eq 1:

$$G = \Delta v_w / \Delta v_s \quad \text{(Eq 1)}$$

Grinding ratios cover a wide range of values ranging from less than one for vanadium-rich high speed steels (Ref 19) to over 60,000 when internally grinding bearing races using cubic boron nitride abrasive wheels (Ref 20). Attempts have been made to address the problems related to the wear of abrasive grains in terms of the theory of brittle fracture (Ref 21). The conclusions of various researchers lead us to believe that the variety of different and interacting wear mechanisms involved, namely, plastic flow of abrasive, crumbling of the abrasive, chemical wear, etc., makes grinding tool wear too complicated to be explained using a single theoretical model (Ref 22). The following analysis of diamond grains represented by single-point loaded wedges assumes that diamond grain fracture is the dominant wear mechanism in a set of grinding tools operating under various grinding conditions. In this study, we show that the addition of nitrogen to methane and hydrogen process gases may be used to influence the surface morphology and structure of the films such that they become suitable for use on microgrinding tools. We also discuss the effects of substrate biasing and abrasion on the nucleation and growth of N-doped diamond films and their influence on the wear of micro grinding tools.

2. Analysis of Stress in a Single-Point Loaded Wedge

Diamond grains are angular and possess sharp cutting points prior to grinding workpiece materials. When deposited on a tool substrate, these grains can be considered to be representative infinite wedges. An infinite wedge represents the cutting point of a diamond grain in contact with the workpiece material (Fig. 1). The wedge is loaded at the apex by a load P in an arbitrary direction at angle ω to the axis of symmetry of the wedge. Resolving the force into components P cos ω in the direction of the axis, and P sin ω perpendicular to that the stresses due to each of these forces can be evaluated from a two-dimensional elastic theory (Ref 23). The state of stress in the wedge, due to force P cos ω, can be obtained from the stress function:

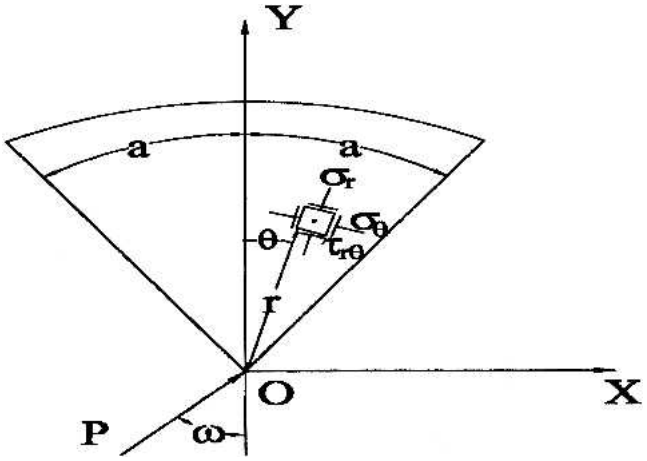

Fig. 1 Single-point, loaded infinite wedge

$$\phi = C\, r\, \theta \sin \theta \quad \text{(Eq 2)}$$

where r and θ are polar coordinates at the point N in Fig. 2, and C is a constant. The stress function yields the following radial, tangential, and shear stress components:

$$\sigma_r = -2C \frac{\cos \theta}{r} \quad \text{(Eq 3)}$$

$$\sigma_\theta = 0 \quad \text{(Eq 4)}$$

$$\tau_{r\theta} = 0 \quad \text{(Eq 5)}$$

To determine the constant C, the equilibrium of forces along the Y-axis is

$$P \cos \omega - \int_a^a \sigma_r \cos\theta \, dA = 0 \quad \text{(Eq 6)}$$

where dA is an element of cross sectional area within the wedge. If t is the thickness of wedge:

$$\cos \omega\, P = \int_a^a 2C \frac{\cos \theta}{r}\, t\, r \cos\theta \, d\theta$$
$$= 2Ct \int_a^a \cos^2\theta \, d\theta = Ct(2a + \sin 2a) \quad \text{(Eq 7)}$$

Therefore,

$$C = \frac{P \cos \omega}{t(2a + \sin 2a)} \quad \text{(Eq 8)}$$

and

$$\sigma_r = -\frac{2P \cos\theta \cos\omega}{r\, t(2a + \sin 2a)} \quad \text{(Eq 9)}$$

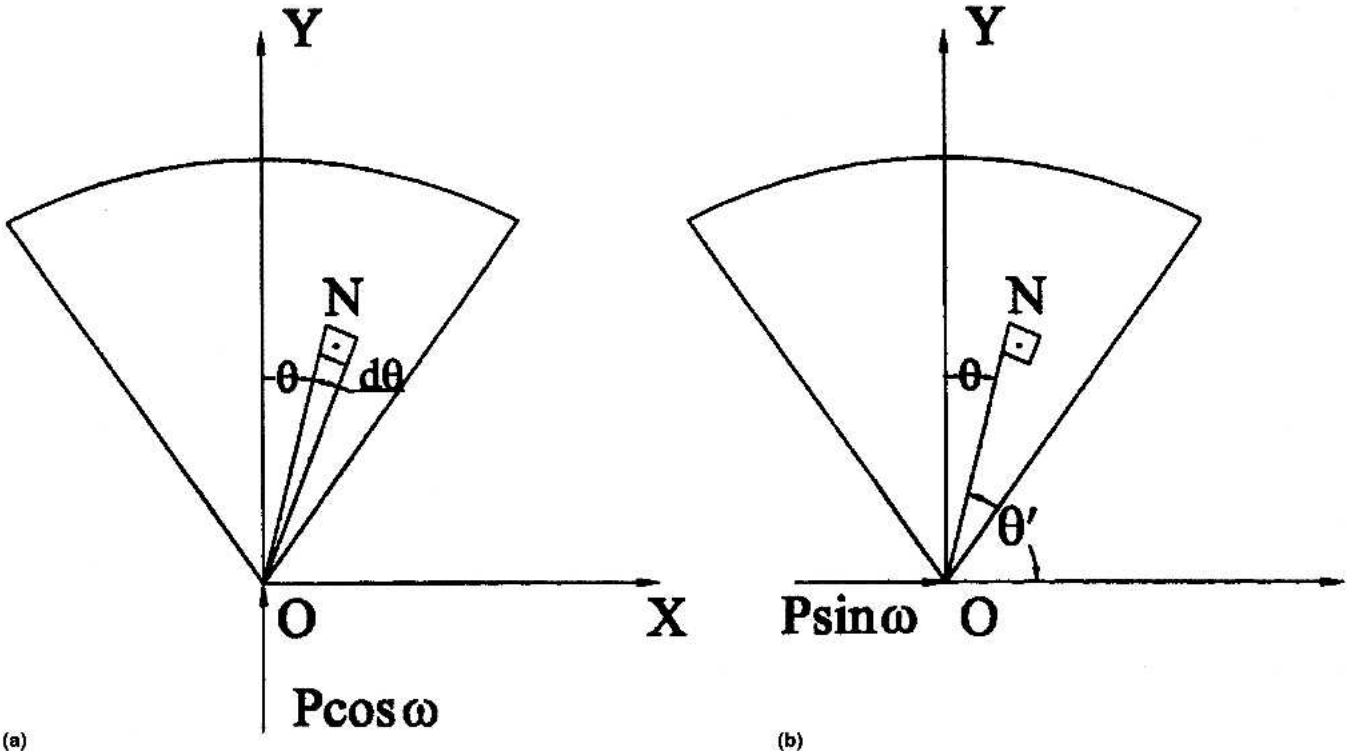

Fig. 2 Single-point, loaded infinite wedge showing force components and the point N within the wedge at polar coordinates r and θ

Note that the negative sign denotes that the stress is compressive in this region. The state of stress in the point-loaded wedge, due to force P sin ω, can be obtained from the following stress function:

$$\phi = C' r \theta' \sin \theta' \quad \text{(Eq 10)}$$

Therefore,

$$\sigma_r = -2C \frac{\cos \theta'}{r} \quad \text{(Eq 11)}$$

and,

$$\sigma_\theta = 0 \quad \text{(Eq 12)}$$

$$\tau_{r\theta} = 0 \quad \text{(Eq 13)}$$

Equilibrium of forces along the X-axis (Fig. 2) yields the following solution for the constant C:

$$P \sin \omega - \int_{\pi/2^{-a}}^{\pi/2^{+a}} \sigma_r t r \cos \theta' d\theta' = 0 \quad \text{(Eq 14)}$$

$$P \sin \omega - \int_{\pi/2^{-a}}^{\pi/2^{+a}} 2C \frac{\cos \theta'}{r} t r \cos \theta' d\theta' = 2Ct \int_{\pi/2^{-a}}^{\pi/2+a} \cos^2 \theta' d\theta' = -C t (2a - \sin 2a) \quad \text{(Eq 15)}$$

$$\therefore C = \frac{P \sin \omega}{t(2a - \sin 2a)} \quad \text{(Eq 16)}$$

Thus,

$$\sigma_r = -\frac{2P \cos \theta' \sin \omega}{r t(2a - \sin 2a)} \quad \text{(Eq 17)}$$

Expressing in terms of the angle θ (where θ′ is negative), yields:

$$\sigma_r = -\frac{2P \cos \theta \sin \omega}{r t(2a - \sin 2a)} \quad \text{(Eq 18)}$$

Therefore, the combined stresses are:

$$\sigma_r = -\frac{2P}{r t}\left[\frac{\cos \omega \cos \theta}{2a + \sin 2a} + \frac{\sin \omega \cos \theta}{2a - \sin 2a}\right] \quad \text{(Eq 19)}$$

It follows that the radial stress σ_r vanishes for angle θ_o defined using the expression:

$$\tan \theta_o = \frac{1}{\tan \omega} \cdot \frac{2a - \sin 2a}{2a + \sin 2a} \quad \text{(Eq 20)}$$

This equation corresponds to a straight line through the apex as shown in Fig. 3. This natural axis separates the regions of compressive and tensile stresses in the wedge. It can be seen that for values of angle ω which gives, $|\theta_o| > |a|$, provides a neutral axis that lies outside the included angle of the wedge. This means that the whole area of the wedge will be under stresses of uniform sign. Expressing Eq 19 in terms of the rake angle of the diamond grain, β, and force components F_t and nF_t (Fig. 3), yields:

$$\sigma_r = -\frac{2F_t}{r t}\left\{\frac{[n \cos(a - \beta) + \sin(a - \beta)]\cos \theta}{2a + \sin 2a}\right.$$

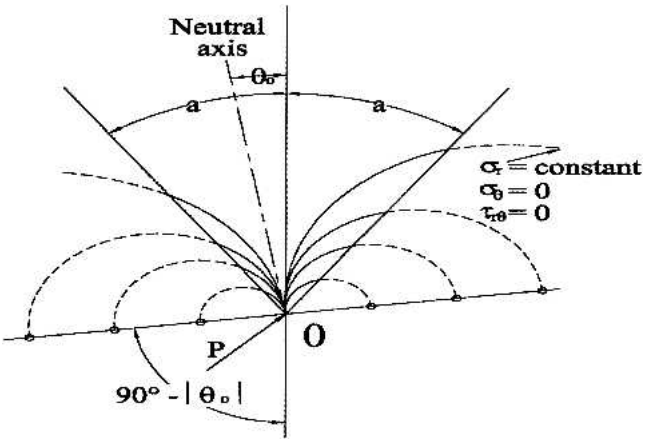

Fig. 3 Stress analysis of a single-point loaded wedge

$$+\frac{[\{\cos(a-\beta)-n\sin(a-\beta)\}\cos\theta]}{2a-\sin 2a}\Bigg\} \qquad \text{(Eq 21)}$$

It is observed that

$$\tan\omega=\frac{\cos(a-\beta)-n\sin(a-\beta)}{n\cos(a-\beta)+\sin(a-\beta)} \qquad \text{(Eq 22)}$$

In the simple case of a wedge with the normal force nF_t along the wedge axis, a is equal to β, hence,

$$\tan\omega = 1/n \qquad \text{(Eq 23)}$$

It is interesting to examine the radial stresses on the left-hand face of the wedge, which corresponds to the leading face of idealised wedge. Thus, for the left-hand face, θ is equal to $-a$, and from Eq 19:

$$\sigma_r=-\frac{2P}{r\,t}\left[\frac{\cos\omega\cos a}{2a+\sin 2a}+\frac{-\cos a\sin\omega}{2a-\sin 2a}\right] \qquad \text{(Eq 24)}$$

This stress is zero, i.e., the neutral axis coincides with the left-hand limit of the wedge, when,

$$\frac{1}{\tan\omega}=\frac{\sin a(2a+\sin 2a)}{\cos a\,(2a-\sin 2a)} \qquad \text{(Eq 25)}$$

Thus if $a = \beta$, then:

$$n=\frac{\sin a}{\cos a}\cdot\frac{2a+\sin 2a}{2a-\sin 2a} \qquad \text{(Eq 26)}$$

$a - \beta = \pi/2 - a$ (as is the case when F_t is parallel to the right-hand face of the wedge).

From Eq 23,

$$\tan\omega=\frac{\sin a-n\cos a}{n\sin a+\cos a}=\frac{\sin a-n\cos a}{n\sin a+\cos a} \qquad \text{(Eq 27)}$$

and substituting in Eq 25 yields:

$$\frac{n\sin a+\cos a}{\sin a-n\cos a}=\frac{\sin a}{\cos a}\cdot\frac{2a+\sin 2a}{2a-\sin 2a} \qquad \text{(Eq 28)}$$

Therefore,

$$\frac{\frac{1}{2}n\sin 2a+\cos^2 a}{\sin^2 a-\frac{1}{2}n\sin 2a}=\frac{2a+\sin 2a}{2a-\sin 2a} \qquad \text{(Eq 29)}$$

$$\frac{1}{2}n\sin 2a(2a-\sin 2a)+2a\cos^2 a-\cos^2 a\sin 2a =$$
$$= 2a\sin^2 a+\sin^2 a\sin 2a-\frac{1}{2}n\sin$$
$$2a(2a+\sin 2a)\frac{1}{2}n\sin 2a(2a-\sin 2a+2a\sin 2a)$$
$$= 2a(\sin^2 a-\cos^2 a)+\sin 2a\; n\; 2a\sin 2a$$
$$= -2a\cos 2a+\sin 2a$$

Hence,

$$n=\frac{1}{2a}-\cot 2a \qquad \text{(Eq 30)}$$

Equation 25 expresses the condition for the whole of the wedge's cross-sectional area to be under the influence of a compressive stress. It can be seen that this depends not only upon the rake angle, β, but also upon the force ratio, n. In general, the relative size of the region of compressive stresses to the region of tensile stresses depends upon β and n as Eq 20 and 22 indicate. Also, from Eq 21, the magnitude of the stress on the left-hand face of the wedge is found to be dependent upon the tangential force component F_t and the force component ratio n. Referring to Eq 19, it can be seen that for constant stress, σ_r = constant:

$$r\,C_1 = C_2\cos\theta + C_3\sin\theta \qquad \text{(Eq 31)}$$

where C_1, C_2, and C_3 are constants. Equation 31 represents, in polar coordinates, the circumference of a circle tangent to the line. Therefore,

$$C_2\cos\theta + C_3\sin\theta = 0 \qquad \text{(Eq 32)}$$

i.e., to the neutral axis at the point when $r = 0$. However, the point $r = 0$ must be considered separately because the stress at that point approaches infinity, since by definition P is a point load. The central point of these circles are of constant radial stress, and so the point of constant maximum shear stress must lie on a line perpendicular to the neutral axis at the point where r is equal to zero. The radius of each of those circles depends upon the magnitude of the radial stress σ_r. Maximum values of stress were computed for a variety of loads and then correlated to the relevant wear parameter, grinding ratio, for a variety of micro grinding tools.

2.1 Development of Wear Model

Brittle materials exhibit high strength properties when loaded in compression than in tension. The ratio of rupture

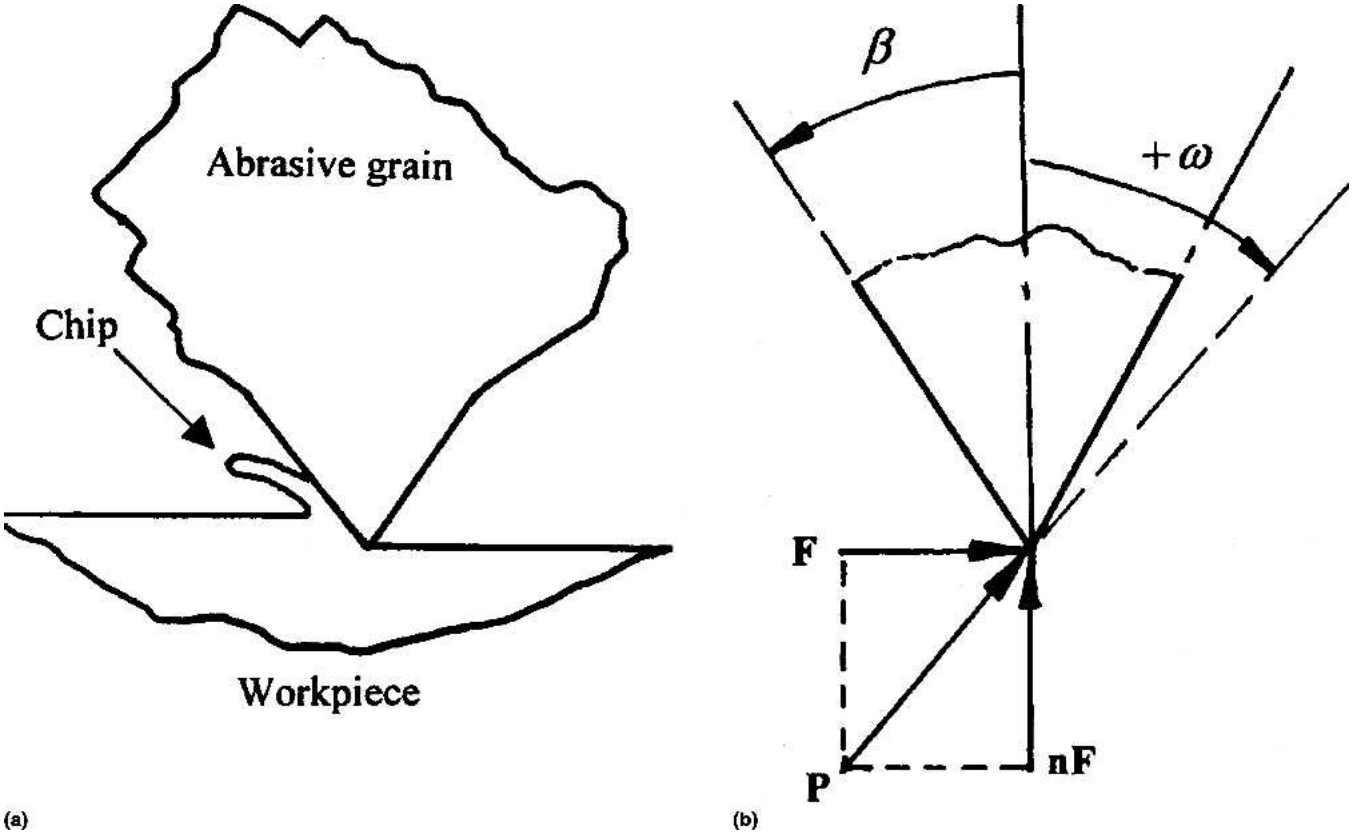

Fig. 4 Ideal wedge-shaped cutting point and grinding force diagram

strengths is usually between 3:1 and 10:1 (Ref 24). The existence of relatively low tensile stresses in the diamond grains may cause failure by fracture to occur. To alleviate fracture, it is possible to use larger grains that reduce the stress levels in the grain when subjected to grinding forces. Changing the amount of nitrogen in the gaseous mixture when creating diamond grains has the effect of changing morphology and the size of grains. Therefore, special attention must be paid to deposition conditions that will optimize the size and shape of diamond grains that will resist negative tensile stresses established in the grains when grinding takes place. Therefore, processing conditions determine the life of diamond grains when subjected to large grinding forces. To measure the effectiveness of the deposition process, it is required to model the effects of tensile stresses on the fracture properties of diamond grains deposited in various gaseous environments to quantify the effects of nitrogen on the life of micro grinding tools.

To model the action of the grinding tool, we must consider a single active cutting point to be classed as a wedge of constant width loaded at its inverted apex with point loads F, and nF, which represent the radial and tangential force components with reference to the grinding tool in which the grain is supported, and P is the resultant force (Fig. 4). The stress distributions within point-loaded wedges can be determined analytically, and the results of such an analysis indicate that if tensile stresses exist within the wedge, it will occur at its maximum along the rake face. The existence of a tensile stress depends on the magnitude of the force ratio n. If the ratio is especially small, such that a tensile stress exists in the wedge, then for a specific force ratio the tensile stress is proportional to the tangential grinding force F. Stresses of this nature would extend to and beyond the diamond grain-substrate interface. The fracture of diamond grain and the interface between the substrate depends on the particular grinding tool used and the magnitude of the tensile stress induced during grinding. Grains of diamond are typically 7-10 times stronger in compression than in tension, and therefore the probability of grain fracture is likely to increase with an increase in tensile stress exerted in the grain, although the magnitude of the stress may be slightly higher than one-fifth the magnitude of the maximum compressive stress in the grain. A significant barrier to the acceptance of stress patterns evaluated for such situations arises because point loads applied to perfectly sharp wedges produce infinitely high stresses at, and about, the point of contact. Therefore, the loads must be applied over a finite area. This implies that compressive stresses dominate over the finite area. Experimental results (Ref 24) show that rake face stresses are compressive over the entire length of chip-tool contact but are tensile outside of this region. The zone of fracture initiation points were located in the tensile zone at about two to two-and-a-half times the chip-tool contact length.

It seems likely that higher tensile stresses are associated with higher grain fracture probability resulting in rapid loss of diamond grains and, consequently, lower grinding ratios. The wear model should incorporate the fact that the loads are spread over a finite area. This implies that single-point loads are resolved into multiple point loads along the rake face, or are indeed, applied directly along the rake face of the cutting tool. The model should allow the relationship between the wear rate of a grinding tool and the general nature of stresses established in active diamond grains subjected to grinding forces to be examined.

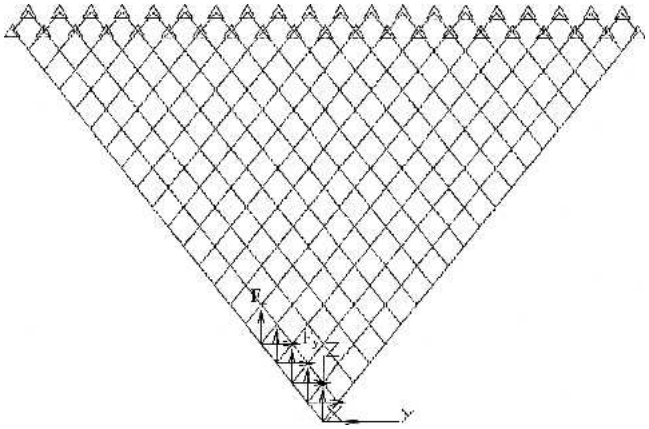

Fig. 5 Finite element assemblage with grinding loads applied at the rake face nodes

2.2 Stress Analysis of Single Diamond Grain

The assumed geometry of an ideal grain in the vicinity of its cutting edge is a simple symmetrical wedge of constant width with an included angle of 70° that results in a rake angle of −35°. There is no wear flat on the model cutting grain. A finite element method is used to evaluate stresses in the wedge, the wedge was subdivided into 210 diamond-shaped elements with a total of 251 nodes. Forty-one nodes were constrained at the boundary of the wedge and the leading five nodes on the rake face were loaded (Fig. 5). The tangential and normal grinding point loads were replaced by a series of multiple loads (F_Y and F_Z) acting perpendicular to (normal load) and along (shear load) the rake face of the wedge.

The loads at the five nodes are representative of the distributed and normal loads acting on the rake face over the diamond grain-chip contact length. The normal force distribution on the rake face was taken as being a maximum value at the cutting edge and decreases linearly to zero at the end of the diamond grain-chip contact length. The shear force was taken to be constant over the first half of the contact length, decreasing linearly to zero over the contact length. Grinding loads were also applied directly to the rake face and at the tip of the diamond without applying multiple loads along the rake face. This was performed to compare and contrast the effect of different force distributions on the stresses generated within the diamond wedge.

To measure the value of using the maximum tensile stress as a way to estimate grain fracture tendency, the correlation between the two sets of data were calculated for each set of data. The region of fracture initiation was also located using Griffith's criterion of fracture (Ref 25), which is applicable to the fracture of brittle materials. For

$$\frac{\sigma_c}{\sigma_t}\sigma_1 + \sigma_3 > 0 \qquad \text{(Eq 33)}$$

Then,

$$\sigma_1 = \sigma_t \qquad \text{(Eq 34)}$$

But for,

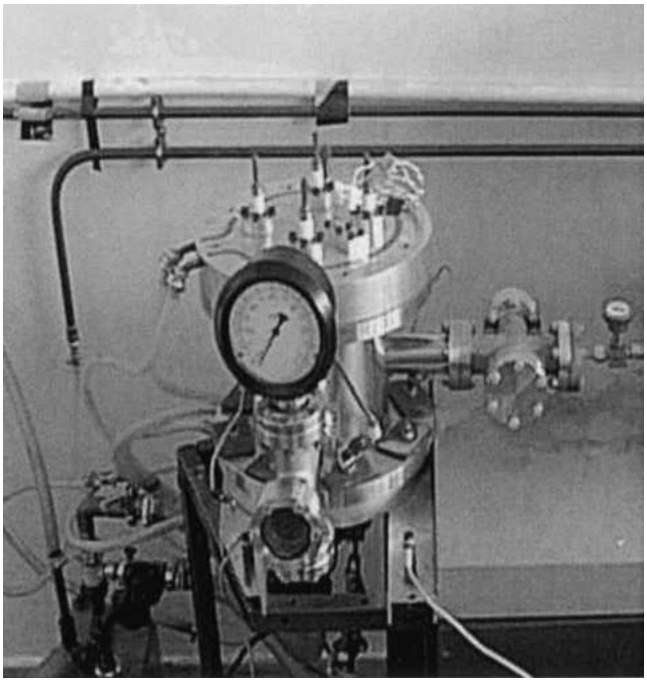

Fig. 6 Hot filament CVD apparatus

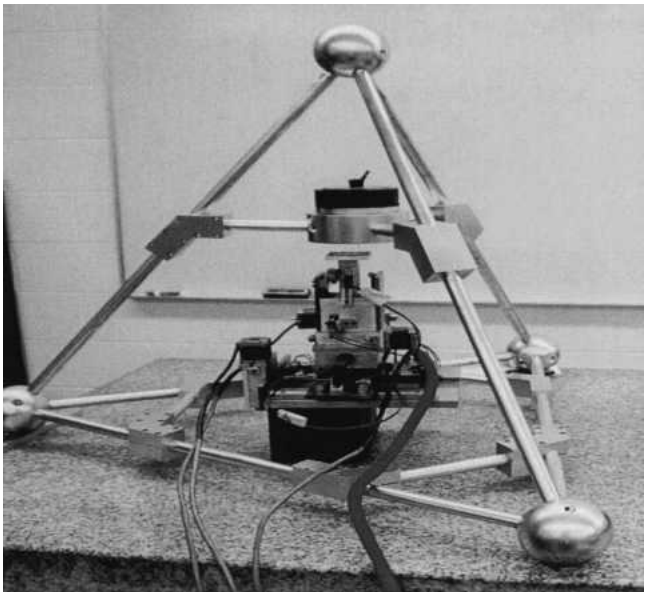

Fig. 7 Micro grinding machine tool showing tetrahedral spaceframe surrounding the precision *x-y-z* table and the extremely high-speed air turbine spindle

$$\frac{\sigma_c}{\sigma_t}\sigma_1 + \sigma_3 < 0 \qquad \text{(Eq 35)}$$

Then,

$$(|\sigma_1| - |\sigma_3|)^2 + 8\sigma_t(|\sigma_1| - |\sigma_3|) = 0 \qquad \text{(Eq 36)}$$

where σ_1 and σ_3 are the principal stresses, assuming that $\sigma_1 > \sigma_3$, σ_t is the ultimate tensile strength of the abrasive grain, and

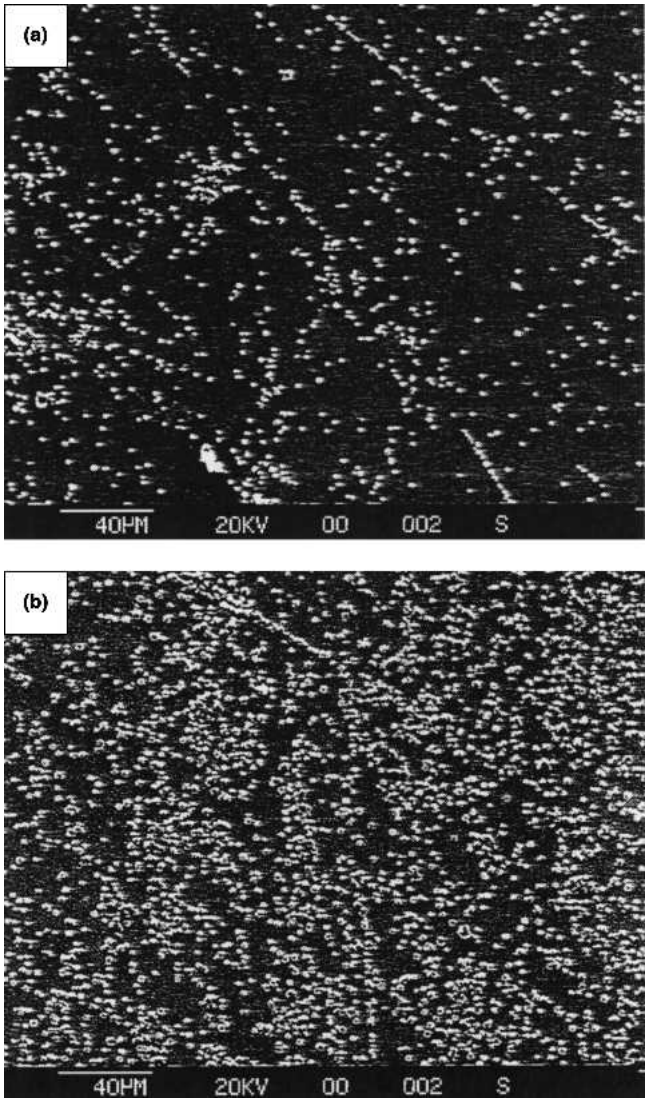

Fig. 8 Diamond nucleation on the unabraded surface prior to deposition for 6 h at 0 and 200 ppm nitrogen addition

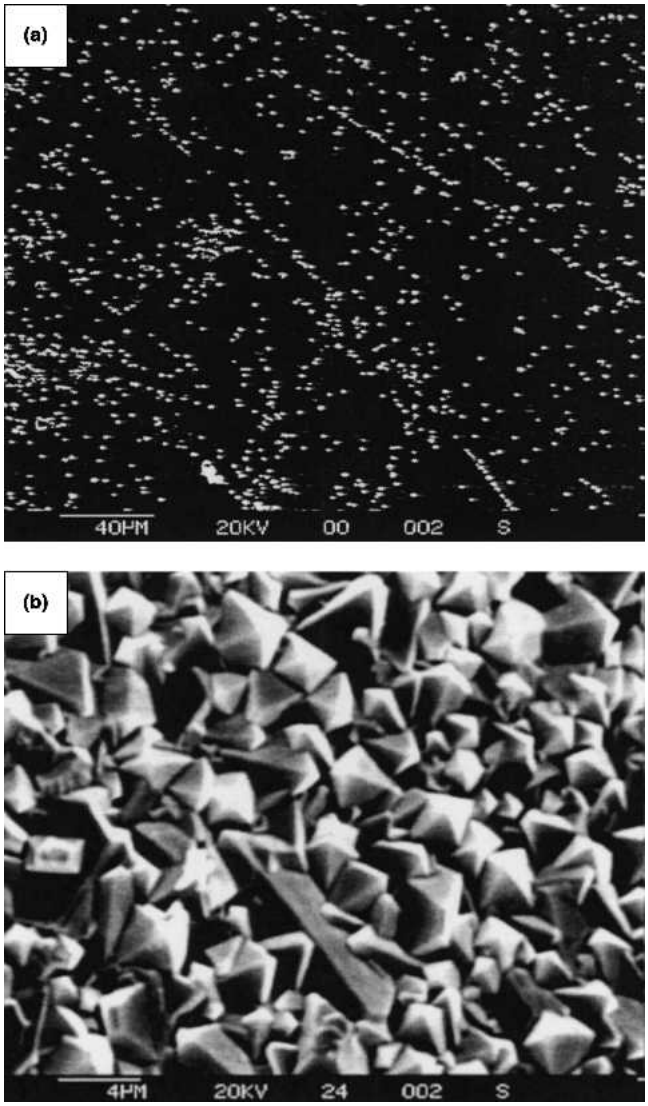

Fig. 9 Diamond growth: (a) without surface abrasion and (b) with surface abrasion with a diamond powder.

σ_c is the ultimate compressive strength. For diamond, the ratio of σ_t and σ_c is approximately 0.1.

3. Experimental Method

3.1 Hot Filament Chemical Vapor Deposition

The hot filament CVD system is composed of a water-cooled stainless-steel vessel, which is connected to a rotary pump enabling a vacuum to be produced. The hot filament CVD apparatus is shown in Fig. 6. Gas flow rates are controlled using MKS mass flow controllers (MKS Instruments, Inc., Wilmington, MA) to accurately control the amounts of gases flowing into the reactor. The system allows independent bias to be applied between the substrate and filament. The filament consisted of a coiled tantalum wire of diameter 0.5 mm to activate the reaction mixture. The filament temperature was measured using an optical pyrometer with values between 2200 and 2500 K. Substrate temperatures were measured using a K-type thermocouple in direct thermal contact with the substrate. After abrasion, the samples were ultrasonically cleaned with acetone prior to deposition. The diamond films were grown on preabraded WC-Co substrates for 4 h under standard deposition conditions (Ref 4). To investigate the effects of changing the gas-phase environment different concentrations of nitrogen, from 50 to 100,000 ppm, were added to the standard 1% methane in hydrogen gas mixture. This is equivalent to varying the N/C ratio from 0.01 to 20. The film morphology, growth rate, and quality were characterized using Raman spectroscopy (Kaiser Holo Probe, 532 nm, Nd: YAG laser, Kaiser Optical Systems, Ann Arbor, MI) and scanning electron microscopy (SEM).

3.2 Measurement of Wear of Diamond Tools

The measurement of the wear of diamonds on a single layer deposited to the grinding tool requires grinding various workpiece materials on a specially constructed machine tool. The machine tool was constructed using a tetrahedral space frame design that attenuates vibrations generated during grinding. The grinding tool is held in an air turbine spindle capable of rotating the grinding tool in excess of speeds of 350,000 revolutions per minute. Figure 7 shows the microgrinding machine tool complete with three axes of motion in the *x*, *y*, and *z*

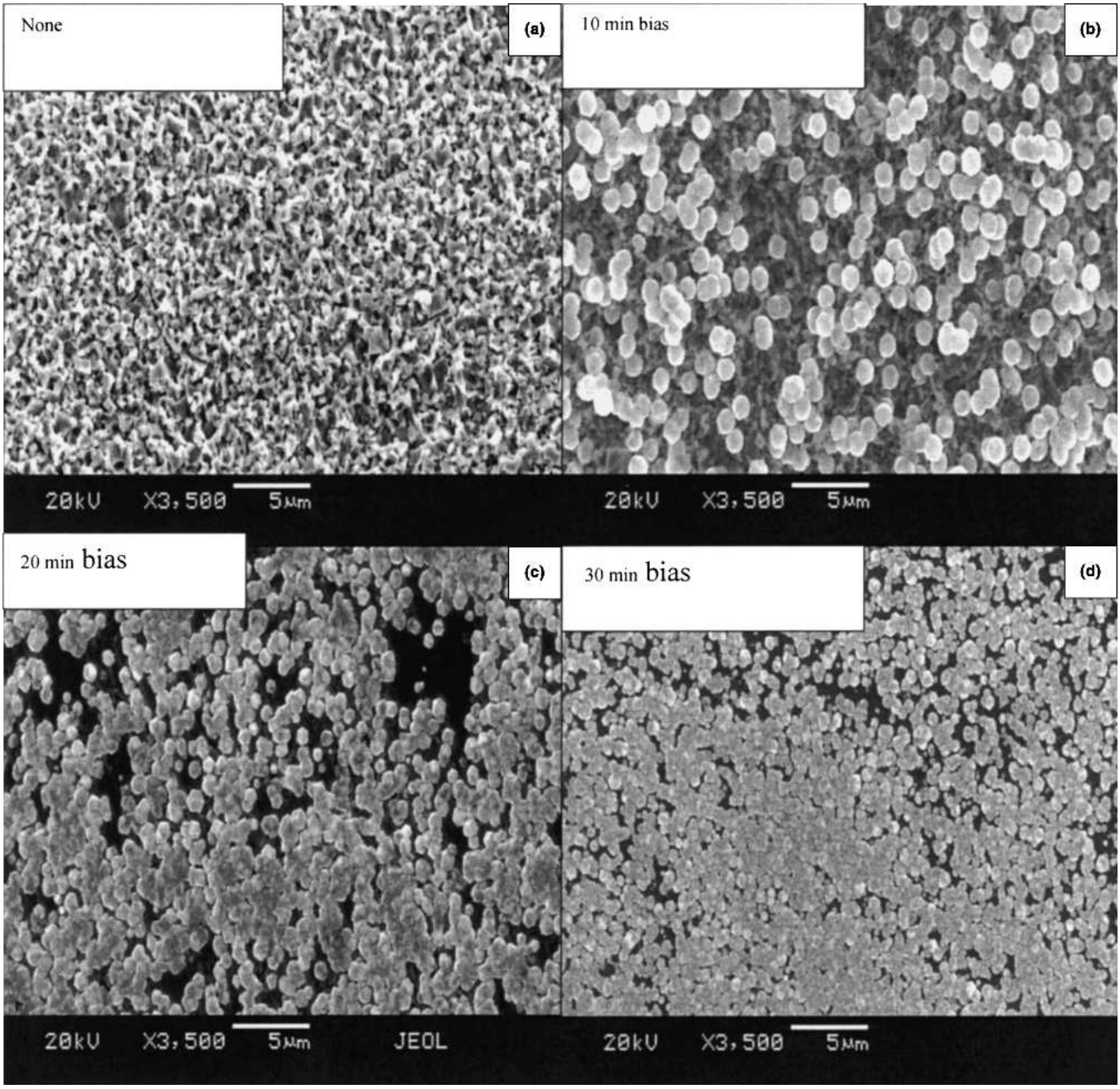

Fig. 10 Scanning electron micrograph showing the effects of biasing time on the nucleation density.

directions. A fourth axis capable of rotary motion can also be used on the machine tool. The machine tool was used to measure the performance of the grinding tools machining materials such as medium carbon steels (hypoeutectoid) and high carbon tool steels (hypereutectoid). Grinding experiments were conducted using a number of grinding tools coated with diamonds that were produced in a hot filament CVD reactor containing gases with varying amounts of nitrogen in a methane/hydrogen mixture. The grinding ratio was measured in accordance with that stated in Sec. 1. However, to correlate the magnitude of tensile stress in the diamond grains to the grinding ratio, it is required to know the number of active cutting grains on the surface of the grinding tool.

The number of active cutting grains on the grinding tool surface is found quite simply by driving a grinding tool into a piece of soft metal that has a length equal to the grinding tool's circumferential length. The depth to which the grinding tool is driven into the length of soft metal is equal to the depth of cut. The impression that the grinding tool produces in the length of soft metal is equal to the number of cutting points that are active during the grinding stroke at that particular rate of cut. However, the grinding tool must be prepared by simulating the grinding conditions used during the experimental conditions. Once the grinding tool has stabilized at its optimum grinding condition, the tool is removed from the machine tool and driven into the soft metal that simulates one grinding revolution into the workpiece material. The force components are then applied to a "model" diamond grain by dividing the grinding force data generated using a dynamometer into the number of active cutting grains over an area that simulates the diamond

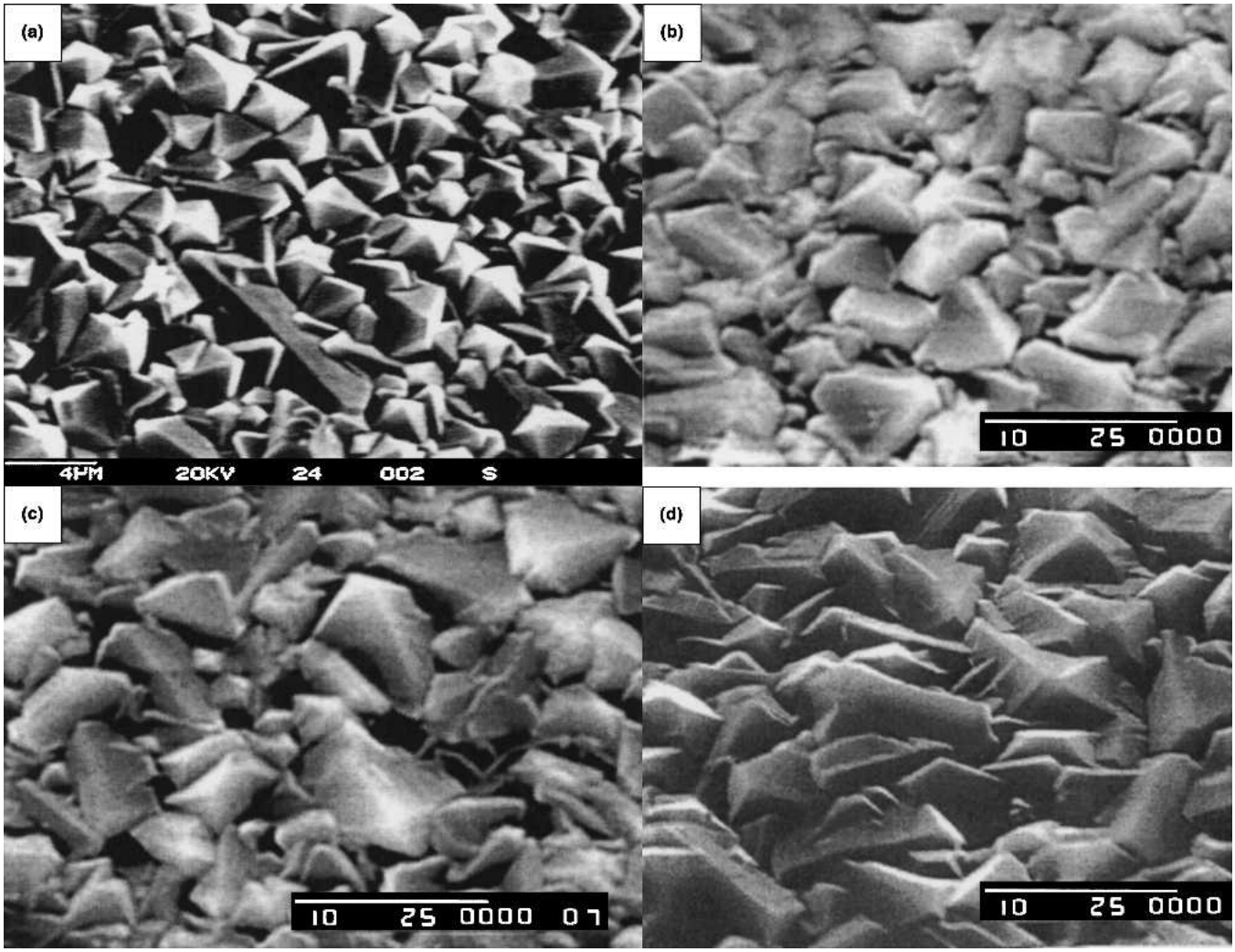

Fig. 11 N-doped CVD diamond growth at 0, 50, 100, and 200 ppm nitrogen

grain-workpiece contact area over one revolution. Stresses established in this area are calculated using finite elements. The wear of the grinding tool, expressed in terms of a grinding ratio, and its relationship to the stresses set up in the model grain are compared.

4. Results and Discussion

4.1 Diamond Deposition

Figure 8 shows CVD diamond growth on unabraded WC-Co substrate for 6 h. A striking increase in diamond nucleation density is observed with the presence of nitrogen in the process gas. It is evident that nitrogen enhances the nucleation of diamond. However, even after 6 h, it not sufficient on its own to cause the growth of a continuous diamond film. Hence, surface abrasion or another form of substrate preparation is necessary in the creation of nucleation sites for the growth of diamond films. Figure 9 shows CVD diamond growth with and without surface abrasion. It is evident that without abrasion even after 4 h of deposition only isolated crystals of diamond appear on the surface of the substrate. However, surface abrasion results in a continuous film of diamond with the nucleation density of about $9 \times 10^8/cm^2$. Mixed crystals of ⟨111⟩ and ⟨100⟩ orientation are formed, which are typically 1-3 μm in diameter. The film is continuous with no evidence of pin-holes or cracks. For micromilling cutting tools, a highly controlled method of surface treatment is desirable. Even though surface abrasion is very effective in creating nucleation sites, it does not allow a high degree of precision and control of surface preparation and therefore bias enhanced nucleation has been investigated as an alternative.

Application of a negative bias of –300 V to the substrate for 30 min prior to the deposition stage gives a measurable increase in the nucleation density with a continuous film forming (Fig. 10). The increase in nucleation is due to the creation of nucleation sites arising from ion bombardment of the substrate. However, at the pressures utilized in this study, 2660 Pa, the mean free path is relatively small and ion acceleration appears unlikely and an alternative explanation may be more likely. Biasing the substrate changes the composition of the plasma creating a higher concentration of hydrogen radicals near to the substrate and therefore the changes in the morphology could be due to a chemical etching effect rather than an ion bombardment effect. It is evident from Fig. 11 that as the amount of nitrogen is increased from 0 to 200 ppm, the size of diamond crystals also increases. The addition of nitrogen is thus enhancing the growth of the diamond crystals. However, the precise

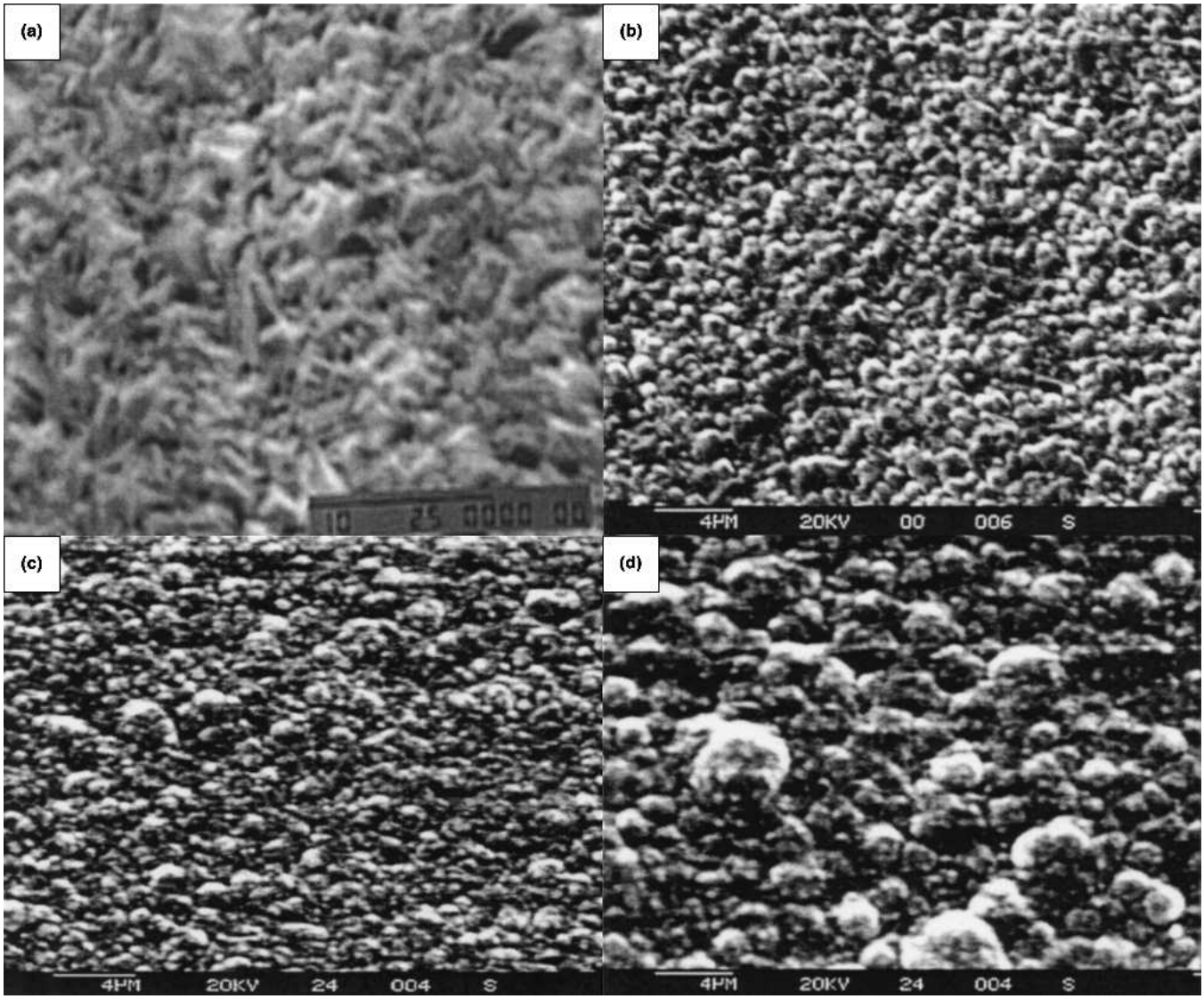

Fig. 12 N-doped diamond at 5000, 10000, 50,000, and 100,000 ppm nitrogen.

reasons for this growth enhancement are still unclear and are being investigated. Figure 12 illustrates that further additions of nitrogen degrade the crystal structure considerably but improves the surface roughness of the films.

These films were grown under the same conditions but in separate studies. The different grain densities indicate the difficulty in obtaining absolute reproducibility, though the relative density measurements are significant. Raman analysis confirms this trend. For relatively small amounts of nitrogen in the gas phase, the full width at half-maximum (FWHM) of the 1332 cm^{-1} absorption characteristic of diamond is reduced indicating an increase in the diamond phase purity. For higher levels of nitrogen, the diamond peak broadens and disappears altogether with N_2 levels above 50,000 ppm in the gas mixture (Fig. 13). This data is consistent with films produced from microwave diamond CVD studies (Ref 8). The changes in the surface morphology and structure are related to the carbon supersaturation, which is controlled by the supply of carbon and the creation of growth sites at the surface (Ref 8). Small amounts of nitrogen are able to reduce carbon supersaturation, which leads to an improvement in crystal quality. At higher levels of nitrogen the carbon supersaturation increases and the morphology changes from blocky to spherical, which is accompanied by deterioration of the diamond phase purity.

4.2 Wear of Diamonds

The wear of microgrinding tools coated with diamonds deposited from various gaseous environments doped with nitrogen appears in Table 1. Here, it is shown that the nature of the diamond is optimised at 200 parts-per-million of nitrogen in methane/hydrogen mixture. Beyond this value, the grinding ratio decreases because the diamonds are becoming smaller in size and the surface is becoming smoother. Below 200 ppm, the diamonds are scattered in random formation producing a discontinuous film of diamonds leaving large areas of the tool unable to grind the surface of the workpiece material.

The results of the two-dimensional stress analyses were consistent with the experimentally determined stress distribution obtained by Loladze (Ref 26) when cutting soft metal with photoelastic tools. The maximum tensile stress always occurs at the rake face at a distance from the cutting edge ranging from

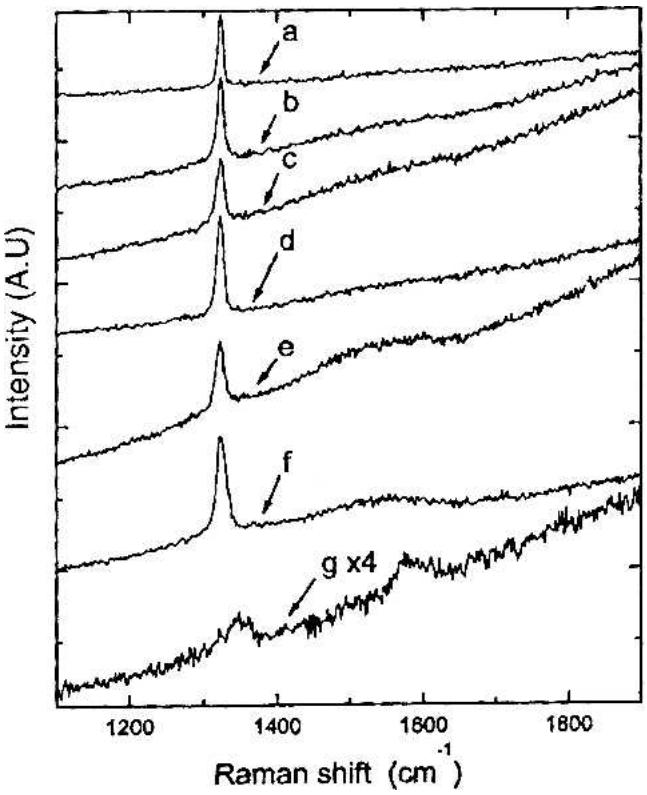

Fig. 13 Raman spectra of N-doped diamond coatings: (a) 200 ppm, (b) 100 ppm, (c) 5000 ppm, (d) 50 ppm, (e) 10,000 ppm, (f) 50,000 ppm, and (g) 0 ppm

1.5 to 4 times the abrasive grain-chip contact length, the exact magnitude of the coefficient depends on the loading conditions for a particular grinding event. For a given value of the tangential force component F and the higher the force ratio F/nF, the greater the distance the maximum tensile stress is away from the cutting edge. These results indicate that mechanically induced fracture occurs at a finite distance away from the cutting edge. When using Griffith's criterion, the influence of mechanically induced stresses indicate that fracture initiation zones are established. Figure 14 shows the occurrence of such zones in an idealized wedge. The first zone is located around the point of maximum tensile stress and is always at the rake face.

Failure in this zone is tensile and would initiate fracture at a point on the rake face of the order of 2-3 times the diamond grain-chip contact length away from the cutting edge. This type of fracture is consistent with fracture on a scale comparable with the chip thickness and tends to produce the so-called "self-sharpening action." The second much smaller zone is located at the immediate vicinity of the cutting edge. Failure is compressive in this region and results in "crumbling" of the cutting edge leading to the formation of a wear flat on the diamond grain.

The correlation between the magnitude of the maximum tensile stress in the model diamond grains and the grinding ratio (Table 2) is high and dependent on the way the forces are applied to the grains. It would be expected that the higher the tensile stress, the greater is the rate of grinding wheel wear and consequently the corresponding grinding ratio. Perfect linear correlation in accordance with this would result in a correlation coefficient of –1. The correlation coefficient between the maximum tensile stress and the grinding ratio is significant. This is to be expected as the force ratio may vary slightly. However, if the tangential component of the grinding force changes significantly without a change in force ratio, it is expected that the maximum tensile stress will change significantly and consequently reduce the grinding ratio.

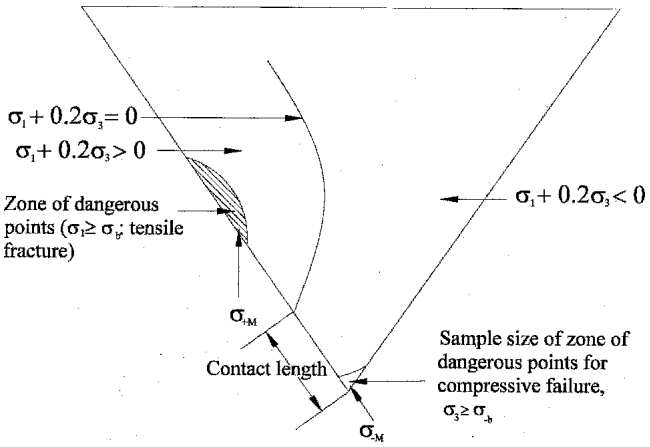

Fig. 14 Griffith's criterion applied to the idealized wedge showing tensile and compressive fracture initiation zones

Table 1 Performance data for grinding normalized M2 tool steel

Nitrogen (ppm in methane/hydrogen mixture)	Grinding ratio
0	50
50	110
100	200
200	300
5,000	175
10,000	85
50,000	60
100,000	20

Grinding conditions: tool diameter, 750 μm; spindle speed, 350,000 rpm; depth of cut, 10 μm; feed rate, 10 μm/min

The calculation and application of multiple grinding loads along the rake face produces a lower correlation coefficient compared with directly applied grinding loads. This implies that grinding loads are simply not point loads acting act the tip of the inverted apex and along the abrasive grain-chip contact length of the grinding grain. In fact, directly applied grinding forces produce better correlation coefficients. This means that for perfectly sharp grinding wheels, one must apply the component grinding loads directly to the rake face.

5. Conclusions

We have shown that the surface morphology of the diamond films can be controlled by employing surface abrasion, substrate biasing, or nitrogen addition to the gas mixture. The application of a bias voltage during normal diamond growth enables renucleation of the diamond film. Thus, the crystal size and surface roughness may be controlled with no reduction in the diamond phase purity. Addition of nitrogen to the gas phase during diamond CVD can also be used to control the surface morphology.

Table 2 Correlation coefficient between maximum tensile stress and grinding ratio for an idealized wedge

Workpiece material	Grinding ratio	Exact wedge model with point loads applied to apex of the wedge	Approximate finite element model: multiple grinding loads applied to rake face of wedge	Approximate finite element model: grinding forces applied directly to the rake face of the wedge
En2 steel (hypoeutectoid	500	–0.7	–0.82	–0.99
Normalized M2 tool steel	300	–0.54	–0.68	–0.98
En8 steel (hypoeutectoid)	250	–0.15	–0.25	–0.6
AISI 52100 (hypereutectoid)	350	–0.76	–0.86	–0.98
Annealed M2 tool steel	250	–0.8	–0.9	–0.99

Wedge simulates a grinding tool that has an optimum diamond coverage using a controlled gas atmosphere of 200 ppm nitrogen in methane/hydrogen mixture. Comparison is also made between the methods of applying loads to the idealized wedge models.

For diamond-coated microtools, grain fracture appears to be the dominant cause of diamond loss during a grinding operation. Grain fracture is much more likely to be caused by mechanically induced tensile stresses within diamond grains than by mechanically induced compressive stresses. The best indicator of microtool performance during a grinding operation under different operating conditions is the level of tensile stress established in diamond grains. High tensile stresses are associated with grain fracture and low grinding ratios in perfectly sharp micro grinding tools. Finite element models of sharp diamond grains can be applied to microgrinding tools where the dominant wear mechanism is grain fracture.

References

1. Q.H. Fan, E. Periera, and J. Gracio, Time Modulated CVD Diamond Processing of Diamond, *J. Mater. Res.,* 1998, Vol 13 (No. 10), p 2787-2794
2. P. May, C.A. Rego, R.M. Thomas, M.N.R. Ashfold, K.N. Rosser, and N.M. Everitt, CVD Diamond Wires and Tubes, *Diamond Relat. Mater.,* Vol 3, 1994, p 810-813
3. L. Kostadinov, D. Dobrev, K. Okano, T. Kurosu, and M. Iida, Nucleation and Growth of Diamond from the Vapor Phase, *Diamond Relat. Mater.,* Vol 1 1992, p 157-160
4. N. Ali, W.Ahmed, I.U. Hassan, and C.A. Rego, Surface Engineering of Diamond Coated Tools, *Surf. Eng.,* Vol 14 (No. 4), 1998, p 292
5. R. Beckmann, W. Kulisch, H.J. Frenck, and R. Kassing, Influence of Gas Phase Parameters on Diamond Kinematics of Thin Diamond Films Deposited by MWCVD and HFCVD Techniques, *Diamond Relat. Mater.,* Vol 1, 1992, p 164-167
6. S.I. Ojika, S. Yamoshita, and T. Ishikura, Diamond Growth on Copper Substrate, *Jpn. J. Appl. Phys.,* Vol 32 (No. 2), 1998, p L1681-L1683
7. W. Muller-Serbert, E. Worner, F. Fuchs, C. Wild, and P. Koidl, Nitrogen Induced Increase in Growth Rate in CVD Diamond, *Appl. Phys. Lett.,* Vol 68 (No. 6), 1996, p 759-760
8. B. Bohr, R. Haubner, and B. Lux B, Influence of Nitrogen Additions on HFCVD Diamond, *Appl. Phys. Lett.,* Vol 68 (No 8), 1996, p 1075-1077
9. W.A. Yarbrough and R. Messier R., Diamond Deposition to Silicon, *Science,* Vol 247, 1988, p 688
10. S.M. Kanetkar, G. Metera, X. Chen, S. Pramanick, P. Tiwari, J. Narayan, G. Pfeiffer, and M. Paesler, Growth of Diamond on Silicon Substrates, *J. Electron. Mater.,* Vol 20, 1991, p 4-11
11. S.D. Wolter, B.R. Stoner, J.T. Glass, P.J. Ellis, D.S. Jenkins, and P. Southworth, Textured Growth of Diamond on Silicon via in situ Carburization and Bias Enhanced Nucleation, *Appl. Phys. Lett.,* Vol 62, 1993, p 1215-1217
12. X. Jiang, C.P. Klages, R. Zachia, M. Hartureg, and H.J. Fuser, Epitaxial Diamond Films on (001) Silicon Substrates, *Appl. Phys. Lett.,* Vol 62, 1993, p 3438-3440
13. F. Stubhan, M. Ferguson, H.J. Fusser, and R.J. Behom, Heteroepitaxial Nucleation of Diamond on Si (001) in HFCVD, *Appl. Phys. Lett*., Vol 66, 1995, p 1900-1902
14. X. Li, Y. Hayashi, and S. Nishino, Analysis of Oriented Diamond Nucleation Processes on Silicon Substrates by HFCVD, *Jpn. J. Phys.,* Vol 36, 1997, p 5197-5201
15. R. Locher, C. Wild, N. Herres, D. Behr, and P. Koidl, Nitrogen Stabilized ⟨100⟩ texture in CVD Diamond Films, *Appl. Phys. Lett.,* Vol 65, 1994, p 34-36
16. S. Jin and T.D. Moustakas, Effect of Nitrogen on the Growth of Diamond Films, *Appl. Phys. Lett.,* Vol 65, 1994, p 403-405
17. T.H. Borst, P.C. Munzinger, and O. Weiss, Characterization of Undoped and Doped Homoepitaxial Diamond Layers Produced by Microwave Plasma CVD, *Diamond Relat. Mater*., Vol 3, 1994, p 515-519
18. S. Koizumi, M. Kamo, Y. Sato, S. Mita, A. Sauabe, and C. Reznik, Growth and Characterization of Phosphorous Doped N-Type Diamond Films, *Diamond Relat. Mater*., Vol 7, 1998, p 540-544
19. L.P. Tarasov, Grindability of Tool Steels, *American Society of Metals*, Vol 43, 1951, p 1144-1151
20. H.K. Tonshoff and T. Grabner, Cylindrical and Profile Grinding with Boron Nitride Wheels, *Proceedings of the 5th International Conference on Production Engineering,* Japanese Society of Precision Engineers, Tokyo, Japan 1984, p 326
21. S. Malkin and N.H. Cook, The Wear of Grinding Wheels—Part 1: Attritious Wear, *Trans. A.S.M.E. J. Eng. Ind.*, Vol 93, 1971, p 1120-1128
22. M.J. Jackson, Vitrification Heat Treatment during the Manufacture of Corundum Grinding Wheels, *J. Mfg. Proc.,* Vol 3, 2001, p 17-28
23. S.P. Timoshenko and J.N. Goodier, *Theory of Elasticity*, 3rd ed., International Student Edition, McGraw-Hill Kogakusha, Tokyo, Japan 1970, p 109-113, 139-144
24. A.G. King and W.M. Wheildon, *Ceramics in Machining Processes* (Academic Press, New York, 1966)
25. A.A. Griffith, The Phenomena of Rupture and Flow in Solids, *Philos. Trans. R. Soc. London,* Vol A221, 1921, p 163-198
26. T.N. Loladze, Requirements of Tool Materials, *Proceedings of the 8th International Machine Tool Design and Research Conference*, Koenigsberger, Ed., Pergamon Press, 1967, p 821-842